

RAPID: An Inexpensive Open Source Dynamometer for Robotics Applications

Nicholas Morozovsky, Robert Moroto, and Thomas Bewley

Abstract—This paper describes the development of an automated dynamometer to characterize brushed direct current motors. The unique mechanical design allows the testing of a wide range of motor sizes. The motor under test is subjected to a given pulse width modulated voltage signal and position, current, and voltage measurements are simultaneously recorded from the integrated sensor suite. An electromechanical motor model is developed by combining the voltage and torque balance equations of the system. A least-squares algorithm is used to estimate the parameters that best fit the observed data to the specified gray box model. The system retains a low cost by using off-the-shelf electronics and cheaply fabricated mechanical parts. The inertia and friction of the system are carefully modeled, removing the need for an expensive torque sensor. The mechanical drawings, electrical schematics, and software are open source and freely available for download. Consistent parameter estimates from a set of high-tolerance and well-documented identical motors demonstrate the accuracy and precision of the system.

Index Terms—Actuator dynamics, dynamometer, friction modeling, parameter estimation.

I. INTRODUCTION

Due to their low cost, wide availability, and simple control implementation, brushed DC motors are desirable actuators for many robotics applications [1], [2]. However, the design process should accurately account for the role of a motor's dynamics. Motor dynamics may potentially be omitted from the system model, but excluding such dynamics can have significant unintended consequences. Robotic systems can experience performance degradation and loss of stability when actuator dynamics are ignored [3]. A potential approach is to assume that the manufacturer's specifications for a given motor are accurate. However, variations in the quality of documentation between manufacturers, often determined from unknown testing procedures, can result in motors whose dynamics are not reflected fully or accurately in the manufacturer's specifications. A motor's specifications may only contain values for one operating point; it may be necessary to operate the motor at, e.g., a different voltage. Moreover, motor specifications do not characterize the motor driver circuit, which operates in conjunction with the motor in actual implementation. Thus, in order to rigorously obtain a reliable actuator model, a given brushed DC motor and motor driver pair can be subjected to empirical testing and subsequent parameter identification.

This paper presents the development of a dynamometer for brushed DC motors and motor drivers which we call the reconfigurable automated parameter-identifying dynamometer (RAPID). RAPID is capable of simultaneously controlling a motor and recording sensor data that are postprocessed to determine the electrical and mechanical parameters of the motor/motor driver system. The entire process is automated, requiring minimal user interaction. RAPID, in Fig. 1, is equipped with a suite of sensors to measure rotational position, current,

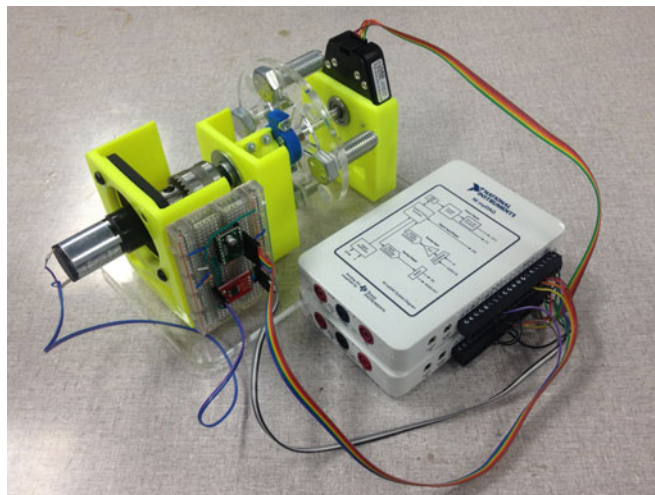


Fig. 1. Dynamometer system.

and voltage. Furthermore, RAPID can accommodate a variety of motor geometries and specifications with its unique hardware design.

The intended application for RAPID is to characterize motors for model-based control systems in robotics applications. Research in the field of dynamometers has been diverse in terms of both the actuators under test and the loading conditions. A small-scale dynamometer has been developed to characterize propeller blades for unmanned air vehicles [4]. This system uses six thin-beam strain gauges to separately measure thrust and torque. The dynamometer developed in [5] has an active braking system designed to simulate different nonlinear loading conditions for the purpose of testing nonlinear control algorithms. A strain gauge measures the reaction torque on the braking assembly. The system was not designed for characterizing different motors. The test setup in [6] that was used to characterize a brushed DC motor with gearbox included a braking system with a rope pulling on a force meter. The sensors were not automatically measured which limited the tests that could be performed on the motor. A dynamometer for miniature piezoelectric actuators was built in [7]. Custom optical sensors measured the deflection of the actuator. Multiple actuators were tested under different operating conditions, but the system is specific to small, bending type actuators. Dynamometers are also used to measure cutting force in machining operations [8]. Strain gauges and piezoelectric sensors are commonly used.

Many of the aforementioned dynamometers (and several others not mentioned) use strain gauges to measure force or torque. Strain gauges require precise calibration and specialized measurement electronics. They must also be carefully mounted in the system to prevent off-axis forces and torques from perturbing the desired measurement. Strain gauges significantly increase the cost and complexity of a dynamometer. For these reasons, we choose not to include a strain gauge.

RAPID consists of off-the-shelf parts, custom parts that may be readily fabricated, and open source algorithms. As such, devices similar or identical to the one discussed in this paper may easily be fabricated for use in many different settings, such as laboratory classes, academic research, and industrial fabrication and quality assurance. RAPID is open source: mechanical drawings and software may be freely downloaded at <http://robotics.ucsd.edu/dyno>.

In this paper, we first review the system design of RAPID, including its mechanical and electrical components. The data acquisition system is then described, including the filtering and postprocessing of various sensors. Next, we develop the equations that describe the electrical and

Manuscript received November 10, 2012; revised April 4, 2013 and June 17, 2013; accepted July 25, 2013. Date of publication August 22, 2013; date of current version December 11, 2013. Recommended by Technical Editor S. K. Saha. This work was supported in part by National Instruments.

The authors are with the Coordinated Robotics Laboratory, University of California at San Diego, La Jolla, CA 92093-0411 USA (e-mail: nmorozov@ucsd.edu; rmoroto@ucsd.edu; bewley@ucsd.edu).

Color versions of one or more of the figures in this paper are available online at <http://ieeexplore.ieee.org>.

Digital Object Identifier 10.1109/TMECH.2013.2276397

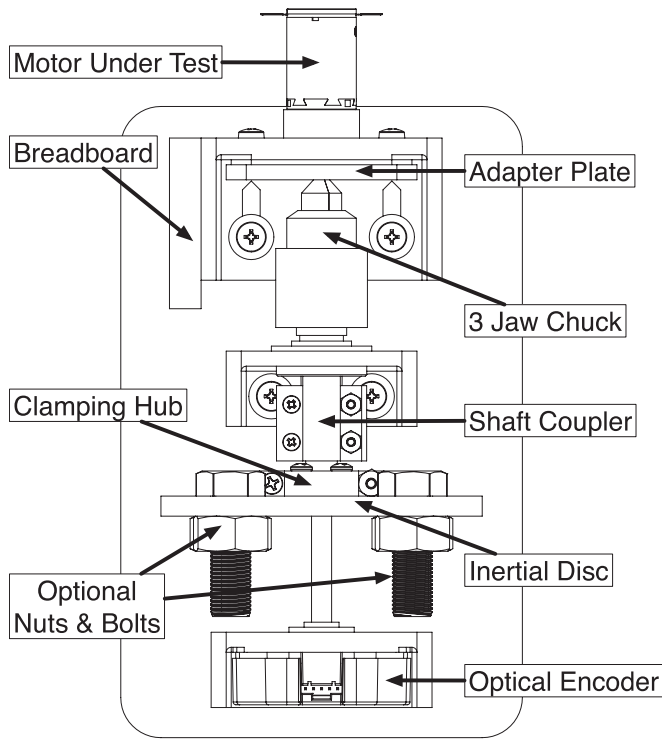


Fig. 2. Labeled overhead drawing of RAPID assembly.

mechanical dynamics of the system, and show how they may be used for gray-box parameter identification. Finally, we present experimental results and summarize our findings.

II. SYSTEM DESIGN

The design of RAPID was driven by two main factors: first, being able to adapt to a wide variety of motors; and second, minimizing the cost and complexity. For ease of use, we impose the requirement that it take less than 15 min to change the motor under test.

A. Mechanical System

The core function of a dynamometer is to exert a known load on the motor under test. To minimize cost and retain simplicity, the load in RAPID is provided by an inertial disc instead of an active or passive braking system. Friction in the system is an additional load on the motor.

Depending on the power of the motor under test, a larger or smaller inertial load is required. In order to accommodate a range of motor specifications, the inertial disc has eight threaded radially-symmetric holes, each capable of holding a single hex head bolt and up to three optional nuts. The removable nuts and bolts can be added in symmetric pairs to the disc to provide 35 different discrete inertial loads between $3.37 \cdot 10^{-5}$ and $1.31 \cdot 10^{-3}$ kg-m² (see Section III).

The inertial disc is rigidly mounted with a clamping hub to an aluminum shaft, which is supported by ball bearings on either end. One end of the shaft is coupled to the rear of a Jacobs three jaw drill chuck, Fig. 2. The jaws of the chuck are used to hold the output shaft of the motor under test. Most motor output shafts possess a round cross section, possibly with a flattened section or a keyway, nominally used to prevent the shaft from slipping. With the drill chuck, RAPID can hold most round shaft cross-sectional shapes so long as they possess three points of contact, 120° apart that are equidistant from the center

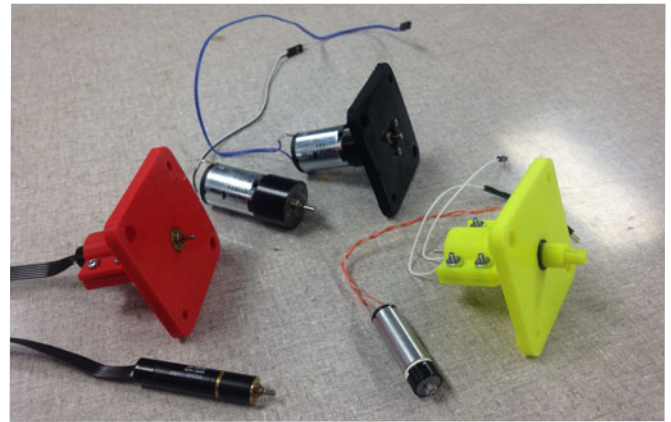


Fig. 3. Adapter plates for three different motors. (center) Face-mounted screws, (left) clamp for round motor housing only, and with (right) added shaft adapter.

TABLE I
ELECTRONICS

Use	Make & Model
Position Sensor	US Digital E6, 2500 CPR
Voltage Sensor	2:3 resistive voltage divider circuit
Current Sensor	Allegro ACS712 ELC-05B-T Hall Effect
Motor Driver	Toshiba TB6612FNG
Data Acquisition	National Instruments myDAQ

of the shaft's rotation. The chuck can accommodate shaft diameters ranging from 1.00 to 6.35 mm (1/4 in). If the output shaft does not meet these requirements, an adapter can easily be made with a 3-D printer that presses onto the output shaft and has a circular protrusion onto which the chuck can grasp. Since the weight of the inertial disc is supported by bearings, there is minimal radial load on the motor shaft.

Different motors may have different mounting features. RAPID is designed to be modular and adaptable. The motor under test mounts to an adapter plate with features specific to the motor, such as face-mounted threaded holes or flat features on the motor body, or the adapter plate may clamp around the entire motor body; see Fig. 3. These adapter plates can be manufactured on a 3-D printer, laser-cutting machine, or other machinery depending on the motor mounting features. A set of modifiable drawings of adapter plates with different common mounting features is available at the aforementioned web site.

B. Electrical System

The electrical system is responsible for delivering power to the motor and measuring several physical values. The sensors, motor driver, and data acquisition device used are listed in Table I. Data are sampled and logged at 100 Hz on all sensors. Two National Instruments myDAQ devices are used to interface the sensors and motor driver over USB with a host computer running LabVIEW software. The two myDAQ devices need not be dedicated to RAPID and can be used for a variety of applications such as a software multimeter or oscilloscope. Other data acquisition devices could also be used by simply adapting the software. The dedicated electronics are all inexpensive.

An optical quadrature encoder is mounted on the end of the inertial disc shaft opposite to the motor under test. By counting the rising and falling edges and comparing the phase delay of the two channels of the encoder, the rotational position can be measured with a precision of four times the resolution of the encoder disc with the counter circuit

on the myDAQ [9]. The encoder disc has 2500 counts per revolution, so the resolution with quadrature is $6.28 \cdot 10^{-4}$ rad. The counter circuit can read a maximum frequency of 1 MHz [10], which corresponds to a maximum rotational speed of 628 rad/s.

RAPID is designed to be compatible with different motor drivers. The motor driver used in the initial testing is listed in Table I and is connected to an external power supply. A pulse width modulated (PWM) 5 V square wave is generated by the timer circuit on the myDAQ [11]. The carrier frequency is 32 kHz and the percent duty cycle is changed at a rate of 100 Hz. The motor driver amplifies the 5 V PWM input signal to the full voltage of the external power supply. The signed duty cycle of the PWM signal (including direction), $\mathbf{u} \in [-1, 1]$, multiplied by the voltage of the power supply V_S is the average voltage across the motor terminals $\bar{V} = V_S \mathbf{u}$. We can not directly measure the voltage across the motor terminals because the PWM carrier frequency is significantly higher than the sampling frequency. Instead, we measure the voltage output of the external power supply, which may be higher than the maximum measurable voltage of the analog to digital converter (ADC), 10 V. We use a simple voltage divider circuit made from off-the-shelf carbon film resistors to step down the voltage. The input of the ADC is connected to an intermediate node of the circuit. The actual voltage can be recovered by multiplying by the ratio of the resistors in the voltage divider circuit. Both the signed PWM duty cycle and power supply voltage are logged, so the average voltage can be calculated by multiplying these two values together.

A current sensor is placed in series between the motor and motor driver. The bandwidth of the sensor itself is 80 kHz, which is more than twice the PWM carrier frequency of the motor driver. However, we are only sampling the sensor at 100 Hz. We implemented a passive first-order low-pass filter with $\omega_c = 93$ Hz in hardware on the output of the sensor to eliminate high-frequency noise from the PWM signal. We limit the maximum frequency of the PWM duty cycle change to well below 50 Hz to ensure there is no aliasing.

The current sensor, motor driver, and voltage divider circuit are mounted to a breadboard mounted on RAPID. A wire harness connects the two myDAQ devices to the breadboard and the encoder. A complete circuit schematic is available at the aforementioned web site.

Some signal processing and filtering must be done before the data can be used for parameter identification. In particular, velocity and acceleration have to be estimated carefully from discrete measurements of position. Any noise in the original data can be exacerbated by numerical differentiation. The high resolution of the encoder disc and quadrature counting minimize differentiation error. We first apply some smoothing to the discrete position data and then use the second-order central difference approximation of the smoothed data to obtain velocity data:

$$\hat{\theta}_k = \frac{1}{6}\theta_{k-1} + \frac{2}{3}\theta_k + \frac{1}{6}\theta_{k+1}$$

$$\omega_k = (\hat{\theta}_{k+1} - \hat{\theta}_{k-1})/2h$$

where h is the sample time, 0.01 s. Combining the previous two equations gives

$$\omega_k = (-\theta_{k-2} - 4\theta_{k-1} + 4\theta_{k+1} + \theta_{k+2})/12h. \quad (1)$$

This formula yields an acceptable estimate of velocity, but the discretization-induced noise is too high to immediately reapply (1) to estimate acceleration. We first apply a 21 time step wide Gaussian filter to smooth out the noise. The window is chosen to be wide enough to smooth the high-frequency discretization and differentiation noise, but not so wide as to eliminate the low-frequency signal of interest. Note that the data are postprocessed such that the filter is centered at the current time step and no phase delay is added. Between the direct

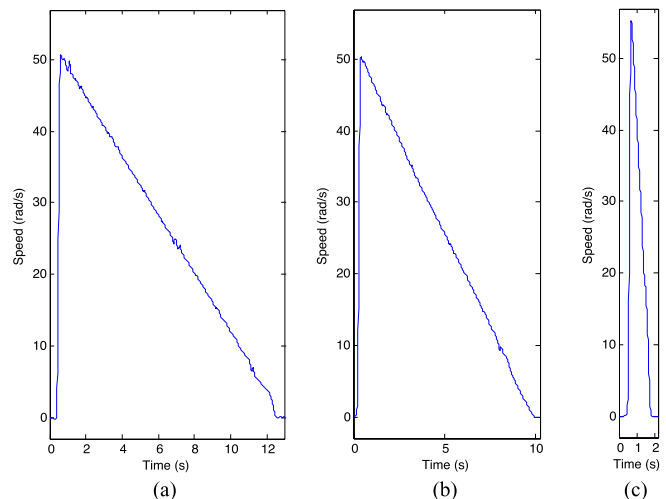


Fig. 4. Results from spin down tests with different loading configurations of inertial disc. (a) Fully loaded. (b) Half loaded. (c) Unloaded.

measurements and the postprocessing, we have calculated values for the velocity, acceleration, average voltage, and current at 100 Hz.

III. SYSTEM MODELING

In order to understand the dynamics of the base system (without a motor installed), we perform multiple spin-down tests. We manually apply an impulse to the system and log the position data as the inertial disc slows to a stop due to friction (see Fig. 4). A total of 44 trials were run, clockwise and counter-clockwise, at different initial speeds, and in three configurations of the inertial disc: fully loaded [8 bolts and 24 nuts, Fig. 4(a)], half loaded [4 bolts and 12 nuts, Fig. 4(b)], and unloaded [0 bolts and 0 nuts, Fig. 4(c)]. The linear slope of the system slowing down demonstrates that Coulomb friction is dominant and viscous and quadratic drag are negligible. We would then expect to be able to model the dynamics with the equation

$$J \frac{d\omega}{dt} = -c \cdot \text{sgn}(\omega) \quad (2)$$

where c is the Coulomb friction coefficient. To verify this model, we performed a simple linear regression for each of the trials. In each case, the coefficient of determination, R^2 , of the linear fit (2) exceeded 0.98, indicating a good fit.

The bearings are the main source of Coulomb friction in the system. Adding nuts and bolts to the inertial disc increases both inertia and weight, which increases the radial load on the bearings, increasing the friction. The friction is not directly proportional to the inertia, otherwise the ratio c/J would be constant and spin down tests with different inertias would have the same slope. This is clearly not the case, as can be seen by the different slopes in Fig. 4. We thus use the following two-term model to characterize the Coulomb friction:

$$c = \alpha + \beta J. \quad (3)$$

Since the nuts and bolts are all added at the same distance from the axis of rotation, the added weight is directly proportional to the added inertia. Thus, the increased Coulomb friction from the increased weight is captured by the βJ term. From (2) and (3), we can solve for the minimum, unloaded inertia of the base system. We call the empirically measured, averaged slopes of the spin-down tests x , y , and z for the unloaded, half loaded, and fully loaded cases, respectively. Using (2)

and noting that the signum function will always be the opposite sign of $\frac{d\omega}{dt}$ for a spin-down trial, we can write

$$\begin{aligned}(J_B)x &= -[\alpha + \beta(J_B)] \\ (J_B + J_N)y &= -[\alpha + \beta(J_B + J_N)] \\ (J_B + 2J_N)z &= -[\alpha + \beta(J_B + 2J_N)]\end{aligned}$$

where J_B is the inertia of the unloaded base system and J_N is the inertia of 4 bolts and 12 nuts. These three equations can be solved for the three unknowns: J_B , α , and β in terms of the known values J_N , x , y , and z :

$$\begin{aligned}J_B &= 2J_N(y - z)/(x - 2y + z) \\ \alpha &= \frac{-2J_N(x - y)(y - z)(x - z)}{(x - 2y + z)^2} \\ \beta &= \frac{2(x - y)(y - z)}{x - 2y + z} - y.\end{aligned}\quad (4)$$

We find $J_B = 3.37 \cdot 10^{-5} \text{ kg}\cdot\text{m}^2$, $\alpha = 1.72 \cdot 10^{-3} \text{ N}\cdot\text{m}$, and $\beta = 2.68 \text{ N}\cdot\text{m}/(\text{kg}\cdot\text{m}^2)$.

With the dynamics of the base system understood, we can proceed to derive equations from first principles that describe the electrical and mechanical dynamics of the motor and base system together. Taking into account the inductance l and resistance r of the motor armature wire, and the back EMF generated when the motor spins, which is equal to the motor constant, k , times the motor shaft velocity, ω , we can write the following voltage balance across the motor terminals:

$$V = l \frac{di}{dt} + ri + k\omega \quad (5)$$

where i is the current through the motor armature wire and V is the voltage across the motor terminals. The torque generated by the motor is

$$\tau = ki \quad (6)$$

where the torque equals the same motor constant k times the current i . The net torque from the motor, subtracting frictional losses, is

$$\tau_N = ki - b\omega - c_M \cdot \text{sgn}(\omega) \quad (7)$$

where b and c_M are the viscous and Coulomb friction coefficients of the motor, respectively. The two equations (5) and (7) form the commonly accepted brushed DC motor model [12]; however, we choose to use a simplified electrical model with the the average voltage and without inductance

$$\bar{V} = ri + k\omega \quad (8)$$

where $\bar{V} = V_S \mathbf{u}$ was defined in Section II-B. The inductance of the armature wire of a small DC motor can be on the order of 10^{-4} H , which is multiple orders of magnitude smaller than the other parameters being estimated. The PWM signal to the motor also increases the frequency of $\frac{di}{dt}$ faster than the sampling frequency. Both of these factors make it difficult to estimate the inductance. The simplified model (8) also allows us to write an equation for the torque generation of the motor (not including frictional losses) as a function of the signed PWM duty cycle $\mathbf{u} \in [-1, 1]$ and speed ω , instead of a function of current as in (6)

$$\begin{aligned}\tau &= \sigma \mathbf{u} - \zeta \omega, \quad \text{where} \\ \sigma &= kV_S/r, \quad \zeta = k^2/r.\end{aligned}\quad (9)$$

The expression for the stall torque, σ , is found by setting $\mathbf{u} = 1$ and $\omega = 0$ in (6) and (8), and solving for τ . The expression for the back

EMF damping coefficient (an electrical term that does not include frictional effects), ζ , can be found by setting $\mathbf{u} = 1$ and $i = 0$ in (6), (8), and (9) and solving for ζ . This is a more useful formulation than (6) because it is more practical to control a motor by voltage PWM (see Section II-B) than controlling current. For these reasons, we choose not to estimate the inductance.

If the motor under test has a gearbox, with reduction γ , the total effective inertia of the motor and gearbox is

$$J_E = J_{\text{Gearbox}} + \gamma^2 J_{\text{Motor}}.$$

The total system inertia J_S includes the minimal base inertia, found in (4), any additional inertia from nuts and bolts added to the inertial disc (known *a priori*), and the inertia of the motor under test

$$J_S = J_B + n_{\text{Bolts}} J_{\text{Bolt}} + n_{\text{Nuts}} J_{\text{Nut}} + J_E. \quad (10)$$

We can write the torque balance of the entire system, starting with (2) and adding the torque of the motor (7)

$$J_S \frac{d\omega}{dt} = ki - b\omega - c_S \cdot \text{sgn}(\omega) \quad (11)$$

where Coulomb friction from the motor and base system are combined into the one parameter c_S

$$c_S = \alpha + \beta(J_S - J_E) + c_M. \quad (12)$$

We subtract the effective inertia of the motor and gearbox, so that the Coulomb friction calculated from the results of the spin-down tests only reflects the inertial disc with any nuts or bolts and all Coulomb friction contributions from the motor are lumped into c_M .

This model is only applicable when the system is in motion, as it accounts for Coulomb and viscous friction, but not stiction. We thus ignore measurements where the velocity is zero. In the general case, Coulomb friction is nonlinear because of the step at zero velocity; however, in this case, we are ignoring data with zero velocity and thus fitting two linear models to the data with nonzero velocity, bypassing the nonlinearity.

Thus, we have (8) and (11) that completely describe the electrical and mechanical dynamics of the motor in RAPID. We use gray-box modeling to find the five unknown parameters of the system: r , k , J_S , b , and c_S that best fit the observed data to the prescribed model [13]. The effective inertia of the motor J_E and the Coulomb friction of the motor c_M can be recovered from J_S and c_S with (10) and (12), respectively.

IV. PARAMETER IDENTIFICATION

To identify the parameters of the motor and driver system, RAPID employs a least-squares algorithm similar to [12]. We define N as the total number of data points taken during a trial and let $f(n)$ denote the value of f at time nh , where h is the sample time of 0.01 s. By the aforementioned construction, the model can be written in matrix form

$$A(n)\mathbf{x} = \mathbf{b}(n) \quad (13)$$

where $\mathbf{x} \in \mathbb{R}^{5 \times 1}$ is the vector of model parameters to be identified. From the set of system equations (8) and (11), we write

$$\begin{aligned}A(n) &= \begin{bmatrix} i(n) & \omega(n) & 0 & 0 & 0 \\ 0 & -i(n) & \frac{d\omega}{dt}(n) & \omega(n) & \text{sgn}(\omega(n)) \end{bmatrix} \\ \mathbf{x} &= [r \quad k \quad J_S \quad b \quad c_S]^T, \quad \mathbf{b}(n) = \begin{bmatrix} \bar{V}(n) \\ 0 \end{bmatrix}.\end{aligned}$$

TABLE II
RESULTS FROM MAXON A-MAX 22 MOTORS

Parameter	Measure	Motor				
		1	2	3	4	5
r	Ω	4.054	3.718	3.745	3.749	3.991
k	$N \cdot m/A$	0.363	0.362	0.357	0.359	0.365
J_E	$kg \cdot m^2$	$1.7 \cdot 10^{-3}$				
b	$N \cdot m/s$	$8.7 \cdot 10^{-4}$	$9.9 \cdot 10^{-4}$	$1.1 \cdot 10^{-3}$	$8.4 \cdot 10^{-4}$	$9.5 \cdot 10^{-4}$
c_M	$N \cdot m$	$3.7 \cdot 10^{-3}$	$4.9 \cdot 10^{-3}$	$6.2 \cdot 10^{-3}$	$5.1 \cdot 10^{-3}$	$5.5 \cdot 10^{-3}$
MSE	V	0.101	0.092	0.099	0.087	0.096
	$N \cdot m$	$2.5 \cdot 10^{-4}$	$2.9 \cdot 10^{-4}$	$2.9 \cdot 10^{-4}$	$2.8 \cdot 10^{-4}$	$2.5 \cdot 10^{-4}$
R^2		0.994	0.994	0.994	0.994	0.993

We further define

$$R_A \triangleq \sum_{n=1}^N A(n)^T A(n), \quad R_{Ab} \triangleq \sum_{n=1}^N A(n)^T \mathbf{b}(n).$$

If we premultiply both sides by $A(n)^T$ and sum over n , we can rewrite (13) as $R_A \mathbf{x} = R_{Ab}$, solving for \mathbf{x} gives $\mathbf{x} = R_A^{-1} R_{Ab}$, so long as R_A is invertible. Whether or not R_A is invertible depends on if the PWM input signal to the motor is sufficiently exciting. For our trials, the percent duty cycle of the PWM signal is given by a sinusoid sweep discretized at 100 Hz. The sinusoid sweep ramps linearly up, then down, in both amplitude (maximum: 6 V) and frequency (from 0.125 to 1.0 Hz). The carrier frequency of the PWM signal does not change, only the percent duty cycle.

We can use different metrics to evaluate how well the identified parameters fit the observed data to the chosen model. Mean squared error (MSE) is the mean of the square of the difference between the observed and estimated data using the identified parameters. The MSE can be calculated separately for the voltage balance (8) and torque balance (11). The coefficient of determination R^2 can be calculated as

$$R^2 = 1 - \frac{\sum_{n=1}^N \epsilon(n)^T \epsilon(n)}{\sum_{n=1}^N \mathbf{b}(n)^T \mathbf{b}(n)}$$

where $\epsilon(n)$ is the residual of the fit, $\epsilon(n) \triangleq \mathbf{b}(n) - \hat{\mathbf{b}}(n) = \mathbf{b}(n) - A(n)\mathbf{x}$.

V. EXPERIMENTAL VALIDATION

We tested five of the same high-quality motor, the Maxon A-max 22 (5 W, 6 V) with a 64:1 spur gearbox [14], [15]. The specifications from this manufacturer are quite detailed and we can thus compare the identified parameters to the specifications to determine the accuracy of RAPID. Comparing the results of the five motors indicates the precision.

The expected torque from this motor is of the order of 10^{-2} N·m, we thus add four bolts to the inertial disc to increase the total inertia. Average results from 20 trials of each motor are shown in Table II. A representative plot of the measured and estimated voltage is shown in Fig. 5 and a plot of both sides of (11) with the estimated parameters is shown in Fig. 6.

The specifications list a k value of 0.377 N·m/A (accounting for the gearbox); the value estimated by RAPID for each of the motors is within 5% of this value. Given that we can expect a manufacturing tolerance of 1–3%, the accuracy of the tests is acceptable. The efficiency of the motor driver may also account for the deviation from the specification, particularly since the values are consistently lower than the specification. The motor driver also affects the estimation of the

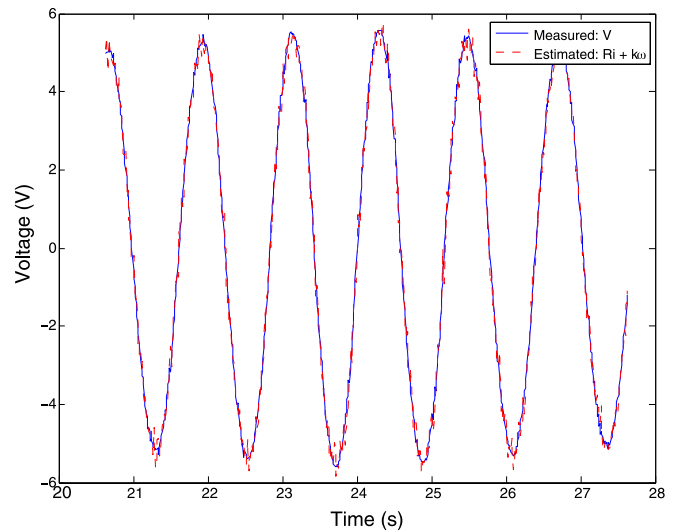


Fig. 5. Measured and estimated voltage [see (8)].

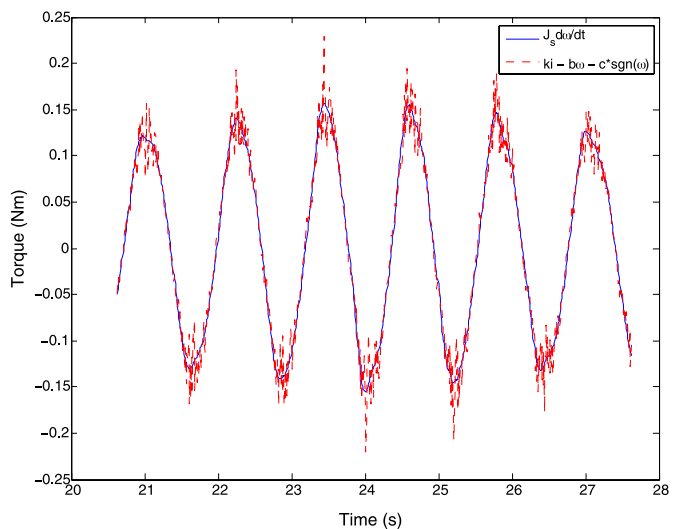


Fig. 6. Torque balance with estimated parameters [see (11)].

resistance of the armature wire. The motor driver H bridge has an “on” resistance on the order of 1Ω , in addition to the resistance in the wire and breadboard. The motor specification is 1.76Ω , which is less than the identified resistance. The estimated effective inertia of the motor and gearbox is within 2% of the specifications. Comparing parameter estimates from motor to motor shows acceptable precision as well. We see the most motor-to-motor variation in the friction parameters. Slight differences in alignment while mounting the motor in RAPID may account for this. MSE values are within 2% of full scale and R^2 values are close to unity and compare favorably with other motor parameter identification results in [12] and [16].

VI. CONCLUSION

An inexpensive, open source dynamometer has been presented that can accurately and precisely fit parameters to a given electromechanical model of a motor. The integrated sensor suite measures several physical values in the system. The reconfigurable mechanical design allows for testing a wide range of motors.

With the motor dynamics identified, a model-based control algorithm may be developed for a robotic system. Future work may include *in situ* testing in a robotic system, using similar algorithms to those developed here, to characterize and track the motor parameters for motor health monitoring as well as estimating external friction parameters, such as rolling resistance over different terrain. Online parameter identification may even be incorporated into the controller [17].

ACKNOWLEDGMENT

The authors would like to thank M. Goeders, M. Kaplan, F. Kharazi, and J. Munoz for help in the design and fabrication of RAPID, and National Instruments and Maxon Motor for their generous support.

REFERENCES

- [1] N. Morozovsky, C. Schmidt-Wetekam, and T. Bewley, "Switchblade: An agile treaded rover," in *Proc. IEEE/RSJ Conf. Intell. Robots Syst.*, 2011, pp. 2741–2746.
- [2] C. Schmidt-Wetekam, D. Zhang, R. Hughes, and T. Bewley, "Design, optimization, and control of a new class of reconfigurable hopping rovers," in *Proc. IEEE Conf. Decis. Control*, 2007, pp. 5150–5155.
- [3] Y. Khaligh and M. Namvar, "Adaptive control of robot manipulators including actuator dynamics and without joint torque measurement," in *Proc. IEEE Int. Conf. Robot. Autom.*, 2010, pp. 4639–4644.
- [4] M. R. Hossain and N. Krouglicof, "Propeller dynamometer for small Unmanned Air Vehicle," in *Proc. 23rd Can. Conf. Electr. Comput. Eng.*, 2010, pp. 1–5.
- [5] Y. Tarte, Y. Chen, W. Ren, and K. Moore, "Fractional horsepower dynamometer—A general purpose hardware-in-the-loop real-time simulation platform for nonlinear control research and education," in *Proc. IEEE Conf. Decis. Control*, 2006, pp. 3912–3917.
- [6] P. Wolm, X. Q. Chen, J. G. Chase, W. Pettigrew, and C. E. Hann, "Analysis of a PM DC motor model for application in feedback design for electric powered mobility vehicles," in *Proc. 15th Int. Conf. Mechatron. Mach. Vis. Pract.*, 2008, pp. 640–645.
- [7] E. Steltz and R. S. Fearing, "Dynamometer power output measurements of miniature piezoelectric actuators," *IEEE/ASME Trans. Mechatronics*, vol. 14, no. 1, pp. 1–10, Feb. 2009.
- [8] G. Totis and M. Sortino, "Development of a modular dynamometer for triaxial cutting force measurement in turning," *Int. J. Mach. Tools Manuf.*, vol. 51, pp. 34–42, 2011.
- [9] Angular Position Measurement with a Quadrature Encoder. [Online]. Available: <https://decibel.ni.com/content/docs/DOC-17346>
- [10] User Guide and Specifications NI myDAQ, [Online]. Available: <http://www.ni.com/pdf/manuals/373060e.pdf>
- [11] Pulse Width Modulation (PWM) Using NI-DAQmx and LabVIEW. [Online]. Available: <http://www.ni.com/white-paper/2991/en>
- [12] S. Saab and R. Kaed-Bey, "Parameter identification of a DC motor: An experimental approach," in *Proc. IEEE Int. Conf. Electron., Circuits Syst.*, 2001, vol. 2, pp. 981–984.
- [13] L. Ljung, *System Identification: Theory for the User*, 2nd ed. Upper Saddle River, NJ, USA: Prentice-Hall, 1999.
- [14] Maxon Motor AG, Motor Specifications, Article Number 110117, [Online]. Available: maxonmotor.com/medias/sys_master/8800973651998/12_097_EN.pdf
- [15] Maxon Motor AG, Gearbox Specifications, Article Number 110483, [Online]. Available: maxonmotor.com/medias/sys_master/8801015988254/12_230_EN.pdf
- [16] J. Stephan, M. Bodson, and J. Chiasson, "Real-time estimation of the parameters and fluxes of induction motors," *IEEE Trans. Ind. Appl.*, vol. 30, no. 3, pp. 746–749, May/Jun. 1994.
- [17] M. F. Moussa, M. Saad, and Y. G. Dessouky, "Adaptive control and on-line identification of sensor less permanent magnet DC motor," in *Proc. IEEE Region 8 Int. Conf. Comput. Technol. Electr. Electron. Eng.*, 2010, pp. 852–857.